JMEPEG (2012) 21:2147–2154
DOI: 10.1007/s11665-011-0116-9

1059-9495/$19.00

Effect of a Strain-Hardening Rate at Uniform Elongation on Sheared Edge Stretching

B.S. Levy and C.J. Van Tyne

(Submitted December 13, 2011)

Edge failure during stretching of sheared edges limits the use of sheet steels in a number of product applications. The shearing process causes a highly strained region adjacent to the shear face, called the shear-affected zone. In the present study, the strain-hardening rate at uniform elongation, *Z*, is used as an empirical measure of cohesive strength at the interface of the various phases in steel microstructures. The higher the value of *Z*, the lower the macro strain when voids begin to form that lead to decohesion of the interface and subsequent failure. The data from four different studies are used to show that the true circumferential strain at failure in a hole expansion is a direct function of *Z* for most microstructural conditions. Sheet steels that exhibit better performance than that which would be expected for their *Z* values have one or more of the following characteristics—an increase in ferrite strength, lower carbon martensite in DP steels, or TRIP steels. A hot-rolled ferrite/pearlite microstructure is the only case of decreased true circumferential strain at failure for a given value of *Z*.

Keywords limit strains during hole-expansion testing, sheared edge stretching, sheet steels, strain-hardening rate at uniform elongation

1. Introduction

Sheared-edge stretching is a two-part process that consists of initial shearing followed by stretching of the sheared edge. Levy and Van Tyne (Ref 1) have shown that variables in production shearing processes include clearance, radii of the shear tools, and angle of the shear blades to the sheet being sheared. In laboratory shearing tests, clearance is typically the only process variable that is evaluated in detail.

The shearing process produces a heavily cold-worked region adjacent to the shear face, which is identified as the shear-affected zone (SAZ). Lee et al. (Ref 2) used grain rotation in the SAZ to calculate shear strains ranging from 1.67 for TRIP 780 to 14.7 for low carbon steel. The strain rate for shearing is probably in the range of 10^3 s^{-1} and is accompanied by substantial adiabatic heating. For these processing conditions, quantitative constitutive equations for deformation in the SAZ are not available. Furthermore, the small size of the SAZ precludes subsequent tensile testing after shearing.

Laboratory stretching tests for sheared edges have been done with flat, spherical, and conical punches with the burr either up or down relative to the punch surface. In production, the tooling for sheared-edge stretching can have even more variation. Deformation rates in laboratory tests are typically slower than in production dies.

B.S. Levy, B.S. Levy Consultants Ltd, 1700 E. 56th St., Suite 3705, Chicago, IL 60637; and **C.J. Van Tyne**, Department of Metallurgical and Materials Engineering, Colorado School of Mines, Golden, CO 80401. Contact e-mail: cvantyne@mines.edu.

Milosevec and Moussy (Ref 3) established that failure in sheared-edge stretching is a ductile fracture process with void nucleation and growth. Milosevic found micro-cracks resulting from shearing.

In deformation at the strains associated with the shearing followed by edge stretching, there must be compatibility between stresses and strains on a macro-level. In contrast, on a micro-scale and in a multi-phase material, the macro-level compatibility may not be fully met. Most commercially available high strength steels are composed of hard and soft phases where the hard phase can be a transformation product, an inclusion, or a precipitate.

To analyze deformation on a micro-scale, experimental determination of the strength of the soft and the hard phases would be required. Experimental efforts to determine the strength of soft and hard phases by micro-hardness or nano-hardness have had varying degrees of success.

Sun et al. (Ref 4) studied the effect of strength of hard and soft phases in DP780 and DP980 steels using synchrotron-based in-situ high-energy x-ray diffraction. Scanning electron microscopy (SEM) analysis was subsequently used to obtain a corresponding two-dimensional finite element analysis (FEA) model. Kim et al. (Ref 5) reported using a realistic, sophisticated approach to determine properties of individual phases for an analysis of sheared edge stretching.

While it is conceptually possible to apply such analytic methods to determine reliable microstructural and stress-strain properties for shearing followed by edge stretching, the work involving these methods is time consuming, requires expensive equipment, and has probably reached the limits of current technology. Such efforts also provide results of uncertain validity. The intent of the present article is to provide an engineering approach for analyzing shearing followed by edge stretching.

As an engineering assumption, at the interface between hard and soft phases, the hard phase deforms elastically, while the soft phase deforms plastically. Sun et al. (Ref 4) has shown that there is no plastic deformation of the hard phase during the deformation of DP780 and DP980 steels. When a hard phase deforms

elastically while a soft phase is deforming plastically, the differences in deformation at a hard phase/soft phase interface are prime locations for micro-void formation, coalescence, and crack formation. Without introducing the complexity of sophisticated failure models, it is intuitive that decohesion at hard phase/soft phase interfaces increases as the strength differential between the hard and soft phases increases. For cases where fracture is within the hard phase, the elastic strains or small plastic strains in the hard phase are sufficient to create stresses that cause failure.

Lee et al. (Ref 6, 7) used a modified measure of strain-hardening rate as a damage parameter in torsion testing. Hudgens et al. (Ref 8) have used a similar approach for evaluating the minimum radius/thickness ratio for bending under tension without fracture. Matlock and Speer (Ref 9) have proposed a similar approach that emphasizes the importance of the strength of the hard and soft phases.

Both the torsion and bending-under-tension tests in Lee et al.'s (Ref 6, 7) and Hudgens et al.'s (Ref 8) studies used as-produced material for which reasonably representative stress-strain data were available for subsequent analysis. In contrast, for shearing followed by edge stretching, the strain in the SAZ is large, so usable stress-strain data are not readily available. Thus, an approximation for the strain-hardening rate is needed. The analysis used in the present study follows the approaches of Lee et al. (Ref 6, 7) and Hudgens et al. (Ref 8) by developing a parameter Z that is hypothesized to be proportional to the strain-hardening rate in the SAZ.

For an incremental increase in strain ($d\varepsilon$) on the macro-scale, the following applies to the soft phase:

$$d\sigma \propto Z\, d\varepsilon \qquad \text{(Eq 1)}$$

where $d\sigma$ is an increment in stress and Z is related to the strain-hardening rate. As Z increases, there is a greater increment of stress for each increment of strain.

The greater the strain in the ferrite, the greater the shear strain at the ferrite/hard phase interphase. There are many failure theories with dominant features of stress, strain, or combinations of stress and strain. For any of these theories, a material with a higher Z-value results in an increase in void nucleation and crack growth that starts at a lower value of macro strain. Hence, for materials with higher Z-values, the failure in a hole-expansion test occurs at lower levels of circumferential strain.

In this study, the parameter Z is taken as the strain-hardening rate at uniform elongation in a tensile test. Uniform elongation is selected because it is the highest strain for which unambiguous stress-strain data are available from a tensile test. The parameter Z also has the advantage that it can be determined from a routine tensile test. This study evaluates the effect of Z on the circumferential strain limit during a hole expansion test.

In calculating Z, Considère's criterion states that the start of local necking in a tensile test occurs when the strain-hardening rate equals the applied stress in the tensile test. For power law hardening, at the uniform elongation strain, the strain-hardening rate and applied stress (i.e., tensile strength as a true stress) are equal when both are expressed as true stress (TS) values. The stress at uniform elongation, which is the point of maximum engineering stress, is the ultimate tensile strength (UTS). The TS at the uniform elongation strain expressed as a function of uniform elongation in percent (%UE) and UTS is

$$\mathrm{TS} = \{1 + (\%\mathrm{UE}/100)\} * \mathrm{UTS} \qquad \text{(Eq 2)}$$

Thus, the true tensile strength equals the strain-hardening rate at the uniform elongation strain. Once necking begins, localization of deformation occurs. There are geometrical effects from the shape of the neck, as well as adiabatic heating effects. Under these conditions, stress-strain relationships are difficult to quantify.

Since the strain-hardening rate at uniform elongation is hypothesized as a measure of decohesion for shearing followed by edge stretching, the literature on cohesive strength between hard and soft phases in sheared edge stretching of various steels is reviewed.

Misra et al. (Ref 10) showed that voids after sheared-edge stretching were observed at ferrite/martensite interfaces. Typically these features are not observed at ferrite/bainite interfaces. Sudo et al. (Ref 11) have reported that the strain to cause void nucleation for ferrite/bainite microstructures is higher than for ferrite/martensite microstructures. Fujita et al. (Ref 12) reported that for steels with higher limit strains in sheared-edge stretching, "the microstructure was controlled to suppress hard carbide formation by lowering its carbon contents and then almost homogenized to a bainite microstructure whose hardness mediated between the soft ferrite phase and the hard martensite phase." Sudo and Kokubo (Ref 13) have also shown that ferrite-bainite-martensite steels have improved limit circumferential strain in sheared edge stretching, as compared with ferrite-martensite steels. Takashashi et al. (Ref 14) have reported that ferrite/bainite microstructures exhibit superior limit strain in sheared edge stretching compared with ferrite/martensite microstructures with reasonably comparable strength. Lee (Ref 15) comments on the superior performance of ferrite/bainite interfaces in sheared edge stretching. Lee (Ref 15) has also shown that a ferrite/carbide interface is weaker than a ferrite/martensite interface.

The results of Misra et al. (Ref 10), Sudo et al. (Ref 11, 13), Fujita et al. (Ref 12), and Takashashi et al. (Ref 14) indicate that a bainite/ferrite interface is more resistant to void formation than a martensite/ferrite interface. These observations are reasonable because bainite is more ductile than martensite and should increase cohesive strength at an interface with ferrite.

Davies (Ref 16) and Fang et al. (Ref 17) have shown the benefit of high strength, high ductility ferrite improving the performance of dual-phase steels. The benefit of increasing the strength of ferrite in a dual-phase microstructure supports the hypothesis that reducing the strength differential at a soft phase/hard phase interface improves sheared-edge stretching.

2. Experimental Data

The experimental data analyzed in this study were consolidated from the results of four separate investigations into a mega study. Mega studies are frequently used in medical research to combine results from multiple investigations to determine a more reliable understanding of the underlying behavior.

2.1 Data of Sriram et al.

Table 1 shows the data from a study by Sriram et al. (Ref 18). The engineering circumferential limit strain in sheared-edge stretching was determined using a conical punch with the burr

Table 1 Data from Sriram et al. (Ref 18)

Steel	Code	Thickness, mm	Tensile strength, MPa	Uniform elongation, %	Strain-hardening rate, MPa	True circumferential strain
DQSK	X-1	0.77	314	21.5	382	0.90
DQSK	X-2	1.19	316	21.0	382	0.92
DDQ+	Y-1	0.70	295	23.8	365	0.92
DDQ+	Y-2	1.19	296	23.5	366	1.02
BH210	B-1	0.70	359	19.3	428	0.92
BH210	B-2	0.93	353	19.0	420	0.92
BH280	C-1	0.71	424	17.9	500	0.69
BH280	C-2	1.00	402	16.0	466	0.69
BH280	C-3	1.04	401	19.5	479	0.70
ULCBH340	D-1	0.74	366	18.0	432	0.95
ULCBH340	D-2	1.02	356	21.2	431	0.80
IF Rephos	E-1	0.63	359	22.0	438	0.88
IF Rephos	E-2	0.89	355	22.2	434	0.95
DP500	G-1	0.66	528	18.9	628	0.44
DP500	G-2	0.81	555	17.4	652	0.45
BH300	1-K	1.24	483	16.5	563	0.51
BH300	2-K	1.19	414	18.5	491	0.81
HSLA350	1-L	1.16	468	19.1	557	0.62
HSLA350	5-L	1.21	501	16.1	582	0.67
HSLA350	2-L	1.62	445	14.6	510	0.64
HS440W	1-M	1.24	483	16.7	564	0.61
HS440W	2-M	1.58	468	16.7	546	0.51
DP600	1-P	0.96	624	16.1	724	0.32
DP600	2-P	1.19	636	15.7	736	0.41
DP600	3-P	1.39	671	16.2	780	0.26
DP600	4-P	1.23	676	13.9	770	0.31
DP600	5-P	1.64	583	18.5	691	0.28
DP600	6-P	1.49	675	13.8	768	0.26
TRIP600	1-T	1.40	673	19.9	807	0.41
TRIP600	2-T	1.60	680	19.3	811	0.34
DP800	1-R	1.20	837	10.7	927	0.20
DP800	2-R	1.59	785	10.5	867	0.17
DP980	1-S	1.15	1037	5.8	1097	0.43
DP980	2-S	1.52	1024	6.0	1085	0.48
RA830	1W	1.32	879	0	879	0.23
RA830	2W	1.53	886	0	886	0.25
RA830	3W	1.25	940	0	940	0.27

up for a wide range of materials. The tests were run at a slow punch speed, and the limit strain was determined by visual observation. Sample size for each material ranged from 3 to 11. The engineering circumferential limit strain reported in the original study was converted to true strain in the present investigation. Levy and Van Tyne (Ref 19) have calculated the average measurement uncertainty for these data to be 0.04.

2.2 Data of Lee

Table 2 shows the results from a study by Lee (Ref 15). These data were analyzed using the same basic test practice as the data from Sriram et al. The sample size for all materials was four. The engineering circumferential limit strain was converted to true strain in this study. The experimental standard deviation for each lot of steel is shown individually.

2.3 Data of Konieczny and Henderson

The hole-expansion tests by Konieczny and Henderson (Ref 20) were run with both conical and spherical punches with the burr both up and down. Clearances of 1.1%, 6.4%, 13.6%, and 20.8% of sheet metal thickness were used in the study. A minimum of three tests were performed for each experimental condition. Failure was determined by stopping the test when a through thickness crack was observed at 3× magnification with good local illumination. The engineering circumferential limit strain was converted to true strain in this study.

Table 3 shows the tensile properties and the limit circumferential strains for the steels in the study. Limit strains are presented for values of a dummy variable (DV). DV equal 0 includes results for the spherical punch with the burr up and down, and the conical punch with the burr up. DV equal 1 is for the conical punch with the burr down. The assignment of a test condition to the dummy variable was based on prior study of Levy and Van Tyne (Ref 19).

2.4 Data of Fang et al.

The tests by Fang et al. (Ref 17) were run using a 50-mm flat punch with a 10 ± 1-mm hole on a 60-ton Erichsen press. The die set for edge stretching used hold down without stingers.

The samples in the study were four commercial hot-rolled steels ranging in thickness from 2.16 to 2.63 mm. Rolling conditions produced either ferrite/pearlite or ferrite/bainite microstructures. Subsequent heat treatments produced a ferrite/bainite or ferrite/martensite microstructure. Metallographic

Table 2 Data from Lee (Ref 15)

Material	Tensile strength, MPa	Uniform elongation, %	Strain-hardening rate, MPa	True circumferential strain average	Standard deviation
Low C	310	23.3	382	0.66	0.04
HSLA	458	15.7	530	0.57	0.04
DP500	603	17	706	0.38	0.04
TRIP590	601	24.8	750	0.33	0.07
TRIP780	814	28.2	1044	0.29	0.02

Table 3 Data from Konieczny and Henderson (Ref 20)

Steel	Thickness, mm	Tensile strength, MPa	Uniform elongation, %	Strain-hardening rate, MPa	True circumferential strain average DV = 0	True circumferential strain average DV = 1
50XK	1.4	488	16	566	0.61	0.73
590R	1.4	621	15	714	0.34	0.46
DP590	1.4	607	16	704	0.37	0.46
DP780	1.4	819	12	917	0.13	0.22
DP980	1.4	985	10	1084	0.07	0.21
TRIP780	1.4	782	19	931	0.15	0.1

DV = 0 includes conical punch burr up and spherical punch burr up and down. DV = 1 is conical punch burr down

Table 4 Data from Fang et al. (Ref 17)

Steel	%C	%Mn	%Si	Strain-hardening rate, MPa	True circumferential strain	Second phase		Estimated strength of ferrite
						Type	%	
As HR								
H1	0.13	0.85	0.07	606	0.313	Pearlite	10	324
H2	0.12	1.34	0.04	648	0.425	Bainite	20	335
H3	0.10	1.20	0.79	680	0.547	Bainite	10	415
H4	0.31	1.51	0.27	813	0.192	Bainite(a)	44	(b)
Ht Tr B								
H1	0.13	0.85	0.07	603	0.445	Bainite	18	324
H2	0.12	1.34	0.04	575	0.470	Bainite	16	335
H3	0.10	1.20	0.79	658	0.547	Bainite	17	415
H4	0.31	1.51	0.27	809	0.219	Bainite(a)	43	(b)
Ht Tr DP								
H1	0.13	0.85	0.07	837	0.170	Martensite	18	324
H2	0.12	1.34	0.04	852	0.229	Martensite	17	335
H3	0.10	1.20	0.79	859	0.297	Martensite	16	415

(a) Strength of ferrite is estimated by the authors to be slightly more than H1 & H2. (b) Mn banding

analysis included volume fraction of hard phase. Tensile tests were run and strain-hardening rate could be calculated from the reported data. Table 4 shows the results.

2.5 Experimental Differences

While the ostensible failure criterion in each study is a through-thickness crack, in practice, this failure criterion is likely to be applied differently. Differences in the application of a through-thickness crack failure criterion can cause significant differences in results between laboratories.

In all the four experimental datasets, the percent hole expansion was measured after samples were removed from the test machine. Once the failure criterion is observed, the test machine is stopped. However, test machines have different inertia that results in additional and variable punch travel after the machine stop button is depressed. Consequently, the hole expands by differing additional amounts before a sample is removed from the test machine. Since hole expansion was measured after the sample was removed from the test machine, different laboratories can produce different values of hole expansion.

It should also be noted that punch inertia generally depends on punch load. Punch load is related to strength and thickness. As stored energy per unit volume increases, the speed of crack propagation increases. The speed of crack propagation may also affect operator observation of a through thickness crack.

When the experimental results within a mega study are analyzed, it can be seen that the results for identical steels can be different. Consequently, in analyzing results from different laboratories, it is necessary to compare trends and recognize that exact matches in results should not be expected.

3. Analysis

3.1 Average Limit Circumferential Strain

Regression analysis is used to determine the effect of strain-hardening rate at uniform elongation on the limit circumferential strain for each individual study. The first step in the regression analysis was to plot the results for each dataset and determine the data points that would fit a linear regression line. Then the regressions for each dataset were run using the data points that would fit a linear regression line. The selection of data points for the regression lines were checked against plots of the results, and the identities of steels that are above or below the regression lines were determined. Several of the steel grades were excluded from the regression analysis. The reason for their exclusion is explained in section 4 of this article.

In order to quantify the increase in circumferential strain for steels above the regression lines, the regression lines were extended to zero limit circumferential strain. For even higher strain-hardening rates, limit circumferential strain is taken as zero.

The square of the correlation coefficient, R^2, is used to show the amount of the total variation explained by each regression. Systematic deviation of data points around the regression lines was qualitatively evaluated. Table 5 gives the regression constant, the coefficient, and the statistics for each of the regression analyses which are described below.

3.2 Results for Sriram et al.'s Data

Figure 1 shows the results for Sriram et al.'s (Ref 18) data, where the dashed lines represent plus or minus one standard deviation. All the steels except TRIP600, DP800, DP980, and RA830 fall on the regression line. The regression constant, coefficient, and statistics are shown in Table 5. It is concluded from more detailed analysis that regression equation is a reasonable description of the experimental data, and that there is no systematic deviation about the regression line.

3.3 Results for Lee's Data

Figure 2 shows the results for Lee's (Ref 15) data, where the experimental standard deviations are shown for each individual data point. Table 5 gives the regression constant, the coefficient, and statistics. Figure 2 and Table 5 indicate that the low carbon, HSLA, DP590, and TRIP 590 steels fit the regression line without systematic deviations. In contrast, TRIP 780 falls above the regression line.

3.4 Results for Konieczny and Henderson's Data

In analyzing the results for Konieczny and Henderson's (Ref 20) data using the average of all four clearances, the regression equation includes a dummy variable (DV) to account for the different deformation processes. An assigned value of zero for DV represents the following processing conditions; the spherical punch with the burr up or down, and the conical punch with the burr up. An assigned value of one represents the conical punch with the burr down.

Figure 3 shows the results for Konieczny and Henderson's (Ref 20) data for the average of all four clearances. Table 5

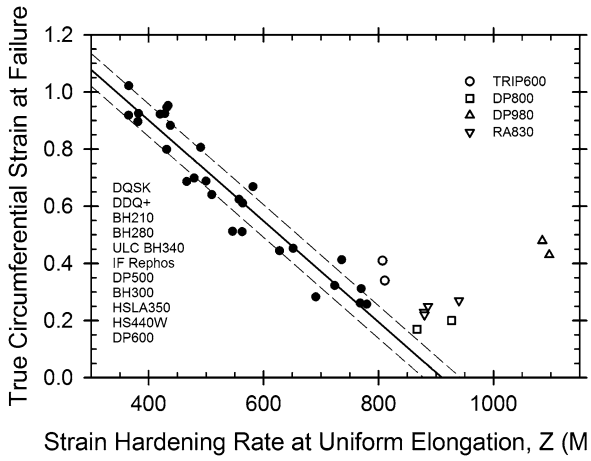

Fig. 1 Effect of strain-hardening rate on the true circumferential strain at failure for Sriram et al.'s (Ref 18) data. The solid data points were used in the regression analysis

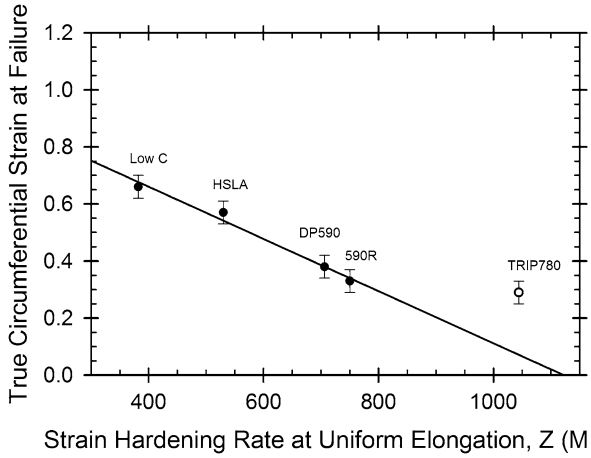

Fig. 2 Effect of strain-hardening rate on the true circumferential strain at failure for Lee's (Ref 15) data. The solid data points were used in the regression analysis

Table 5 Comparison of regression results

Dataset	Constant	Standard deviation	Strain-hardening rate		Dummy variable		Sample size	R^2
			Coefficient	Standard deviation	Coefficient	Standard deviation		
Sriram et al. (Ref 18)	1.61	0.06	−0.0018	0.00010	NA	NA	28	0.92
Lee (Ref 15)	1.03	0.05	−0.0009	0.00008	NA	NA	4	0.98
Konieczny and Henderson (Ref 20)	1.28	0.05	−0.0012	0.00007	0.095	0.022	20	0.95
Fang et al. (Ref 17)	1.18	0.04	−0.0012	0.00006	0.165	0.127	9	0.99

gives the regression constant, the coefficient, and statistics. It can be seen from Fig. 3 and Table 5 that the 50XK, 590R, DP590, and DP780 steels are represented by the regression equation and that the dummy variable provides a reasonable description of the different deformation processes. However, some systematic variation can be observed. It can also be seen from Fig. 3 that the DP980 steel is slightly above the regression line.

Close examination of the results for DV equal zero and one show that for the higher strength steels, the difference between DV equal to zero and one decrease with increasing strength. This result is expected because Levy and Van Tyne (Ref 1) have shown previously that the difference between burr up and burr down for a conic punch decreases as strength increases, and that there is no effect of burr position for a spherical punch.

3.5 Results for Fang et al.'s Data

In visual examination of Fang et al.'s (Ref 17) data, it was observed that the key difference in results was the strength of the ferrite. The regression equation in this study uses a dummy variable that equals zero for low strength ferrite and one for higher strength ferrite. It was also observed that the ferrite/pearlite sample exhibited a low circumferential limit strain for its strain-hardening rate and that the ferrite/martensite sample for H2 exhibited anomalous behavior.

The regression equation was run excluding the ferrite/pearlite and the anomalous H2 ferrite/martensite sample. It can be seen from Fig. 4 and Table 5 that the regression equation is an excellent fit to the experimental data used in the regression analysis, and that there is no systematic deviation about the regression line.

4. Discussion of Results

4.1 Comparison of Regression Results

Figure 5 shows the four datasets plotted on a single graph. There is an overall general trend of a decrease in the limit circumferential strain as Z increases. The wide scatter in the trend is due to the different test practices used in the four individual studies. Although this general trend is interesting, to determine definitive effects of microstructures on the limit strain, the results of the four studies need to be analyzed individually.

Table 5 shows the regression results for the four datasets, where it can be seen that regression statistics are excellent.

The regression results show that the true circumferential strain at failure is predicted by the strain-hardening rate at the uniform elongation, Z, for a wide range of steel grades and microstructures. Phenomenologically, Z is a measure of the cohesive strength between hard and soft phases. The regression results apply to microstructures with a relatively soft ferrite and the following hard phases—angular or spherical carbides, some pearlite, titanium carbonitrides, bainite, and higher carbon martensites. Steel grades with these microstructures in this study include DDQ + , DQSK, IF Rephos, BH210, BH280, BH300, ULC BH340, HSLA350, and related steels, HS440W, 590R, DP500, and DP600.

The regression equations provide a base line against which other steel grades and microstructures can be compared. The hot-rolled pearlite microstructure falls below the regression line. DP780 is borderline—one data point fitting the regression line and one data point above the line, which suggests that the

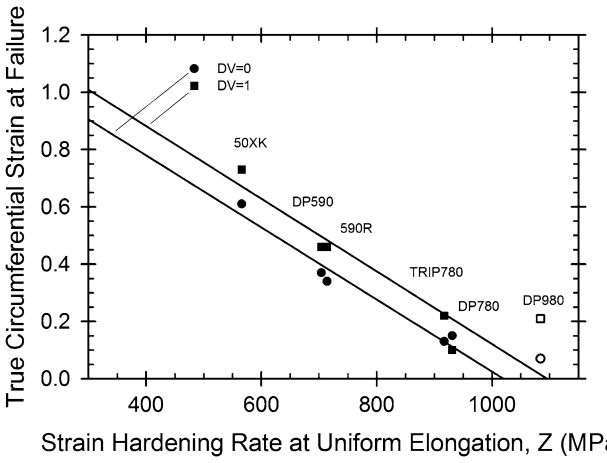

Fig. 3 Effect of strain-hardening rate on the true circumferential strain at failure for Konieczny and Henderson's (Ref 20) data. The solid data points were used in the regression analysis

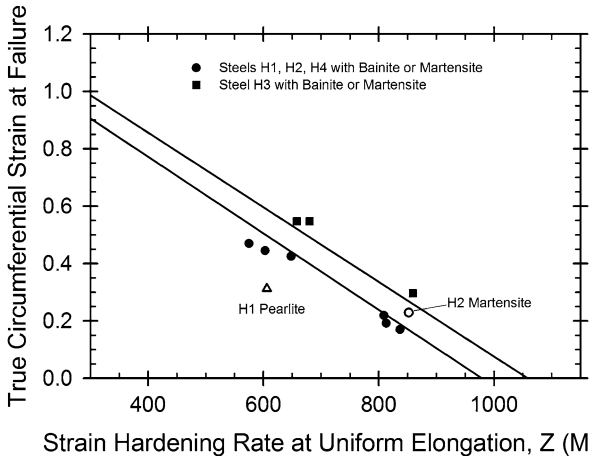

Fig. 4 Effect of strain-hardening rate on the true circumferential strain at failure for Fang et al.'s (Ref 17) data. The solid data points were used in the regression analysis

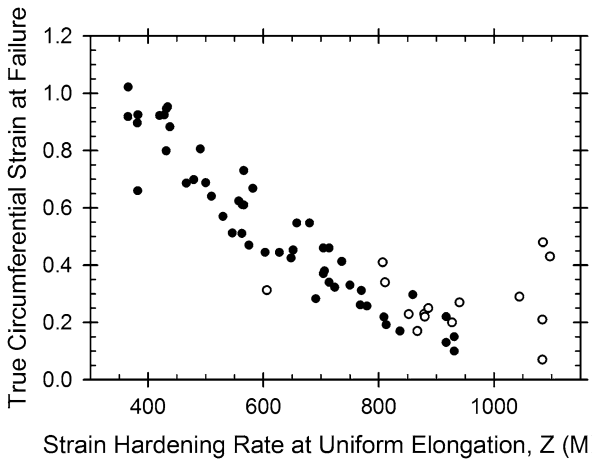

Fig. 5 Effect of strain-hardening rate on the true circumferential strain at failure for the combined datasets

ferrite/martensite interface for DP780 is at the border line of applicability for the base regression. Steels with microstructures that are more resistant to cohesive failure at a given value of Z include DP800, DP980, TRIP590, TRIP600, TRIP780, and RA830. The following sections discuss the nature of these deviations.

4.2 Effect of Bainite Versus Martensite

The ferrite/martensite microstructures in Fang et al.'s (Ref 17) study are for higher strength dual phase steels. Fang et al.'s (Ref 17) results show that contrary to the reported literature, ferrite/bainite and ferrite/martensite steels exhibit similar behavior when corrected for the strength of the ferrite.

Sriram et al.'s (Ref 18) data and, to a lesser extent, those of Konieczny and Henderson (Ref 20) show that the higher strength ferrite/martensite microstructures exhibit improved limit circumferential strain compared to the base line data in these studies. In higher strength dual-phase steels, the volume fraction martensite is greater, but the carbon content of the martensite is lower. Since the shear strength differential between a lower carbon martensite and ferrite is less than for higher carbon martensite and ferrite, it is reasonable to conclude that, at a constant strain-hardening rate, the cohesive strength between the lower carbon martensite and ferrite should be greater.

4.3 Effect of TRIP Steels

Lee's (Ref 15) data show that the single TRIP 780 steel in the study exhibits superior cohesive strength over single samples of low carbon steel, HSLA, DP590, and 590R steel. In contrast, for Konieczny and Henderson's (Ref 20) data, the single TRIP steel exhibits similar or slightly lower limit circumferential strain than the other steels in the study. Given the variation in production methods for TRIP steels, some differences in behavior can be expected.

4.4 Effect of Ferrite Strength

It can be seen from Sriram et al.'s (Ref 18) data that at a value of Z, the limit circumferential strain for the RA830 steel is considerably higher than for the base line data. RA830 is a recovery-annealed steel. After recovery annealing, the strength of the ferrite is much higher than after conventional annealing. As a result, the strength differential at ferrite/carbide interfaces is much less than for fully annealed ferrite/carbide interfaces.

The regression result for Fang et al.'s (Ref 17) data uses a dummy variable to evaluate the effect of increasing ferrite strength in increasing limit circumferential strain at similar values of strain-hardening rate for ferrite/bainite and ferrite/martensite interfaces. The coefficient of the dummy variable shows that increasing the estimated ferrite strength from a nominal tensile strength of about 330-415 MPa increases limit circumferential strain by 0.16.

4.5 Effect of Pearlite

In Fang et al.'s (Ref 17) study, there is a single pearlite sample that exhibits a limit circumferential strain well below the value of the base line regression at a similar value of Z. In the analysis of Sriram et al.'s (Ref 18) study for a tandem reduced product, it is shown that steels with ferrite/pearlite microstructures fit the base line regression. In Fang et al.'s (Ref 17) study, the comparison steels are hot-rolled and have ferrite/bainite or ferrite/lower carbon martensite. It is hypothesized that pearlite in a hot-rolled product can have different microstructural characteristics than for heat-treated, tandem-reduced product.

4.6 Deformation Process

It can be seen from Konieczny and Henderson's (Ref 20) data that the relationship between strain-hardening rate at uniform elongation and limit circumferential strain is valid for different deformation paths. As an engineering approximation, it can be concluded that strain path in the SAZ is different for sheared edge stretching with a conical punch compared to a spherical punch. The results of the regression for Konieczny and Henderson's (Ref 20) dataset validate that limit circumferential strain for any given deformation process is a direct function of Z.

Sriram et al. (Ref 18) have shown that there is a linear relation between limit circumferential strain with a flat punch and a conical punch. Given the linear relation, it can be inferred that there should be a linear relation between strain-hardening rate at uniform elongation, Z, and limit circumferential strain for a flat punch.

Given the available evidence, it appears that the relation between strain-hardening rate and limit circumferential strain is applicable to any specific deformation path and burr position. The effect of deformation path or burr position affects the constant and/or the slope of the regression relation.

5. Summary

- The strain-hardening rate at uniform elongation, Z, is a measure of cohesive strength for a wide range of microstructures. Since true circumferential strain at failure in a hole-expansion test depends on the cohesive strength between hard and soft phases, Z predicts true circumferential strain at failure for microstructures included in the base line regression equation.
- Where the strain-hardening rate at uniform elongation predicts the true circumferential strain at fracture, it is shown that when corrections are made for different deformation conditions in laboratory hole expansion tests, the base regression results apply.
- Steels with increased true circumferential strain at fracture for a given value of Z exhibit the following characteristics—an increase in ferrite strength, and lower carbon martensite in DP steels or TRIP steels.
- A hot-rolled ferrite/pearlite microstructure is the only case of decreased true circumferential strain at failure for a give value of Z.

References

1. B.S. Levy and C.J. Van Tyne, Review of the Shearing Process for Sheet Steels and Its Effect on Sheared Edge Stretching, *J. Mater. Eng. Perform.*, 2011, doi:10.1007/s11665-011-9997-x
2. S.B. Lee, J.G. Speer, Matlock, and K.G. Chin, Analysis of Stretch-Flangability Using a Ductile Fracture Model, *Proceedings of 3rd International Conference on Advanced Structural Steels*, H.C. Lee, Ed. (Seoul, Korea), Korean Institute of Metals and Materials, 2006, p 841–849
3. Z. Milosevec and F. Moussy, Simulation of sheared edge behavior in stretch flanging by a modified Fukui test, *Advanced Technology of*

Plasticity, Vol II, K. Lange, Ed., Springer-Verlag, Berlin, Germany, 1987, p 697–702
4. X. Sun, K.S. Choi, W.N. Lui, and M.A. Khaleel, Predicting Failure Modes and Ductility of Dual Phase Steels Using Plastic Strain Localization, *Int. J. Plast.*, 2009, **25**, p 1888–1909
5. J.H. Kim, M.G. Lee, D. Kim, D.K. Matlock, and R.H. Wagoner, Hole-Expansion Formability of Dual Phase Steels Using Representative Volume Element Approach with Boundary-Smoothing Technique, *Mater. Sci. Eng. A*, 2010, **527**, p 7353–7363
6. S.B. Lee, J.G. Speer, and D.K. Matlock, The Influence of Phase Distribution and Interfaces on Fracture and Formability of High Strength Steel Sheets, *Proceedings of International Conference on Advanced High Strength Sheet Steels for Automotive Applications* (Warrendale, PA, USA), AIST, 2004, p 383–394
7. S.B. Lee, D.K. Matlock, and J.G. Speer, Ductile Fracture Criteria Based on Damage Accumulation Rate, *Proceedings of 19th Conference on Mechanical Behavior of Materials* (Seoul, Korea), Korean Institute of Metals and Materials, 2005, p 183–197
8. A.W. Hudgins, D.K. Matlock, J.G. Speer, and C.J. Van Tyne, Predicting Instability at Die Radii in Advanced High Strength Steels, *J. Mater. Process. Technol.*, 2010, **210**, p 741–750
9. D.K. Matlock and J.G. Speer, Design Considerations for the Next Generation of Advanced High Strength Steel Sheets, *Proceedings of 3rd International Conference on Advanced Structural Steels*, H.C. Lee, Ed. (Seoul, Korea), Korean Institute of Metals and Materials, 2006, p 774–781
10. R.D.K. Misra, S.W. Thompson, T.A. Hylton, and A.J. Boucek, Microstructures of Hot-Rolled High-Strength Steels with Significant Differences in Edge Formability, *Metall. Mater. Trans. A*, 2001, **32A**, p 745–759
11. M. Sudo, S. Hashimoto, and S. Kambe, Niobium Bearing Ferrite-Bainite High Strength Hot Rolled Steel with Improved Formability, *Trans. Iron Steel Inst. Jpn.*, 1983, **23**, p 303–311
12. N. Fujita, T. Nonaka, T. Tomoko, H. Taniguchi, K. Goto, and K. Yamazaki, Development of Ultra-High Strength Steel Sheets with Tensile Strength of 980 MPa, SAE Paper No. 2007-01-0341, *Steel Innovations, Fatigue Research, Sheet/Hydro/Gas Forming Technology & Advanced High Strength Steel Development*, SP 2103, SAE International, Warrendale, PA, USA, 2007, p 51–55
13. M. Sudo and I. Kokubo, Microstructure-Mechanical Property Relations in Multi-Phase Steel, *Scand. J. Met.*, 1984, **13**, p 329–342
14. T. Takashashi, O. Kawano, Y. Tanaka, and M. Ohara, Fracture Mechanical Study on Edge Flangability of High Tensile Strength Sheet Steels, *Steel Processing, Product, and Applications Symposium at MS&T* (Warrendale, PA, USA), TMS, 2009
15. S.B. Lee, "Microstructural Influences on the Fracture Behavior of Multi-Phase Sheet Steels," Ph.D. dissertation, Colorado School of Mines, Golden, CO, USA, 2005
16. R.G. Davies, Influence of Silicon and Phosphorus on the Mechanical Properties of Both Ferrite and Dual Phase Steels, *Metall. Trans. A*, 1979, **10A**, p 113–118
17. X. Fang, Z. Fan, B. Ralph, P. Evans, and R. Underhill, The Relationships Between Tensile Properties and Hole Expansion Property of C-Mn Steels, *J. Mater. Sci.*, 2003, **38**, p 3877–3882
18. S. Sriram, C. Wong, M. Huang, B. Yan, and D. Urban, *Formability Characterization of a New Generation of High Strength Steels*, Report No. 0012, American Iron and Steel Technology Roadmap Program Office, Pittsburgh, PA, USA, 2003
19. B.S. Levy and C.J. Van Tyne, Failure During Sheared Edge Stretching, *J. Mater. Eng. Perform.*, 2008, **17**, p 842–848
20. A. Konieczny and T. Henderson, On Formability Limitations in Stamping Involving Sheared Edge Stretching, SAE Paper No. 2007-01-0340, *Steel Innovations, Fatigue Research, Sheet/Hydro/Gas Forming Technology & Advanced High Strength Steel Development*, SP 2103, SAE International, Warrendale, PA, USA, 2007, p 41–50